

# Imaging of Stellar Surfaces with the Navy Precision Optical Interferometer

Anders M. Jorgensen<sup>a</sup>, H. R. Schmitt<sup>b</sup>, G. T. van Belle<sup>c</sup>, D. J. Hutter<sup>d</sup>, J. Clark<sup>b</sup>,  
D. Mozurkewich<sup>e</sup>, J. T. Armstrong<sup>b</sup>, E. K. Baines<sup>b</sup>, S. R. Restaino<sup>b</sup>

<sup>a</sup>New Mexico Institute of Mining and Technology, Socorro, NM, USA

<sup>b</sup>Naval Research Laboratory, Washington, DC, USA

<sup>c</sup>Lowell Observatory, Flagstaff, AZ, USA

<sup>d</sup>Naval Observatory Flagstaff Stations, Flagstaff, AZ, USA

<sup>e</sup>Seabrook Engineering, Seabrook, MD, USA

## ABSTRACT

The Navy Precision Optical Interferometer (NPOI) is a unique observatory that is especially well-suited for interferometric imaging. The key features are an array layout that includes equally, or nearly equally-spaced stations, the ability to observe with 6 telescopes simultaneously, the beam-relay system flexibility that allows the 6 observed stations to be placed in a chain-configuration, the reconfigurability that allows the telescopes to be moved, and wide wavelength coverage at visible wavelengths. The chain-configuration makes baseline bootstrapping possible, where the fringes are stabilized on very long baselines far below the fringe-tracking signal-to-noise ratio level and thus obtain high-resolution observations. The reconfigurability and flexibility makes it possible to obtain complete Fourier (UV) coverage in only a few nights of observations. The wide visible wavelength coverage has several advantages. First, many stars have high-contrast surface features at visible wavelengths. Second, the wide wavelength coverage makes wavelength bootstrapping possible in which fringe-tracking on short baselines at longer wavelengths can be used to phase observations on long baselines at shorter wavelengths in order to further increase the resolution. In this paper we describe the NPOI Stellar Surface Imaging project, funded by the National Science Foundation, and show one important result that is the bootstrapping of a 5-telescope chain, a feat that has not been achieved at any other interferometer.

## 1. INTRODUCTION

Stars are small, often a few milliarcseconds in diameter, or less. Imaging stellar surfaces requires aperture diameters of sometimes hundreds of meters. In general, the diffraction limited angular resolution of an aperture,  $\theta$ , is inversely proportional to the diameter of the aperture,  $D$ , and proportional to the wavelength being observed,  $\lambda$ ,

$$\delta\theta \sim \frac{\lambda}{D}. \quad (1)$$

There are many practical complications of large apertures, ranging from the mechanical problems of building and supporting large mirrors to the computational and controls problems of flattening the wavefront from atmospheric turbulence and flexing of the large structure.

An alternative approach now being used increasingly widely in astronomy is the synthetic aperture imaging technique that uses many small apertures spread out over an area whose diameter equals the desired aperture diameter for the imaging. With a suffi-

ciently large number of telescopes the imaging resolution now goes as the maximum telescope separation,  $L$ , rather than the individual aperture diameter,

$$\delta\theta \sim \frac{\lambda}{L}. \quad (2)$$

The diameter of the individual apertures no longer determine the imaging resolution. An interferometer does not produce a direct image on a CCD as do traditional telescopes. Instead the light is piped to a central beam combining facility where the beams are interfered. The amplitude and phase of the interference patterns, the visibility, are Fourier components of the image of the object being observed. In principle an image can then be reconstructed by measuring the Fourier image and inverse Fourier transforming it. In practice the process of imaging reconstruction is more involved, but it is well-established in radio interferometry, and a number of different techniques have been developed for image reconstruction in the optical regime.

Interferometric imaging requires several technologies that we will describe in the following section, in-



**Figure 1.** Aerial photograph of the NPOI. The three arms of the interferometer are marked by the surrounding road and the relay pipes can be distinguished. The four astrometric stations are seen as four white buildings near the array center, and a number of imaging stations are shown as white marks along the arms. Up to 6 imaging stations can be populated with siderostats at a time.

cluding a appropriate observatory layout and a data acquisition system tailored to the types of observations, as well as specific data processing techniques.

The capabilities that are being developed as part of the NPOI Stellar Surface Imaging Project are also key to interferometric observations and imaging of near-Earth space objects. Such observations are not the topic of this paper, but interferometric satellite observations are a topic that the authors of this paper have addressed elsewhere.<sup>1–8</sup>

## 2. INSTRUMENTATION

The stellar surface imaging project relies on two sets of hardware that we describe here.

### 2.1. The Navy Precision Optical Interferometer

The Navy Precision Optical Interferometer<sup>9</sup> (NPOI) is a collaboration between the Naval Observatory, the Naval Research Laboratory, and Lowell Observatory. The NPOI consists of 4 fixed siderostats that can be used for astrometric observations, and 6 movable imaging siderostats. NPOI can observe with any 6 siderostats simultaneously, and baseline lengths can be

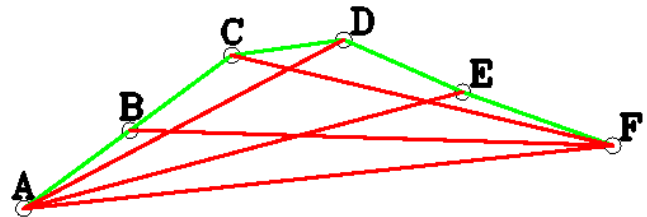


**Figure 2.** NPOI baseline bootstrapping scheme. NPOI can observe up to 6 stations at a time. By placing these 6 stations in a linear configuration and tracking fringes on the high-SNR short connecting baselines it becomes possible to observe on the long resolving baselines.

adjusted by moving the imaging stations along the three arms of the Y-shaped array, from less than 20 m to more than 400 m. Figure 1 is an aerial photograph of the NPOI. The image shows the four astrometric siderostat huts as well as beam relay pipes.

A key capability of the NPOI is baseline bootstrapping. It is possible to configure imaging and astrometric siderostats such that long baselines are composed of chains of stations. Because NPOI can observe up to 6 siderostats simultaneously it can support baseline chains of up to 6 siderostats. This represents the longest bootstrapping chain of any interferometer current or

past.

The original data acquisition and fringe-tracking system of the NPOI is now often referred to as the Classic system. It consists of three spectrographs each with 32 avalanche photodiodes that provide wavelength coverage from 850 nm to 450 nm nominally. Each spectrograph accepts up to 4 of the 6 beams, resulting in a total of 18 pairwise interference patterns being recorded simultaneously (with 3 redundant). Thus all baselines are recorded. However because the data acquisition system was originally designed for a simpler instrument setup it does not record all data all the time or track baselines as needed to take full advantage of the array configuration for imaging. This necessitated a new data acquisition system.

## 2.2. The New Classic Instrument

The New Classic instrument is a back-end upgrade to the NPOI Classic beam combiner. It uses the same detectors and pulse transmission circuit as the Classic system. However, the data collection, storage, and processing are different. New Classic delivers several new capabilities. It is capable of recording data continuously from all three spectrographs versus the Classic system that has the capacity to record only one-third of the channels at a low duty cycle. It incorporates a large amount of computing power that permits more sophisticated fringe-tracking algorithms. In particular long baseline bootstrapping becomes possible. This is in contrast to the Classic system that, due to limited computing power, is limited to bootstrapping at most three stations at a time. This new capability means that the NPOI can take full advantage of its baseline bootstrapping capability and make observations on long baselines that resolve the star.

Imaging requires long baselines that resolve the target, but fringe-tracking generally requires short baselines that have larger fringe-tracking signal-to-noise ratio (SNR). The baseline bootstrapping solution, as illustrated in Figure 2 make is possible to take advantage of larger SNR on the short baselines to track fringes. When the short connecting baselines are locked on fringes, the longer baselines (e.g. A-D or A-F) are also locked on fringes even though those fringes are undetectable on the short fringe-tracking time-scale, typically milliseconds. However by recording data for a long period of time (seconds to minutes) those weak fringes can be brought out from the noise background, and processed coherently with phase information in a post-processing step.<sup>10–12</sup>

## 2.3. Fringe-tracking algorithm

Next to the capability for continuously recording all data, the fringe-tracking capability of the New Classic instrument is the most important. The New Classic fringe tracker is organized as three separate sections: (1) the delay detector, (2) the state-machine, and (3) the combinatorial engine. Figure 3 shows a top-level schematic of the fringe-tracker.

The delay detector detects the presence of a fringe, including an estimation of the delay and a SNR. This calculation is done separately for each baseline being tracked. The group-delay calculation currently implemented in the delay detector allows for any coherent integration of the raw data, incoherent integration of the group-delay power spectrum, and smoothing of the estimated delay and SNR. The resulting delay and SNR information for each tracked baseline, is then passed to the state-machine.

As Figure 3 shows there is also one state-machine for each tracked baseline. The delay and SNR estimate for the baseline is used to update the state. In the New Classic default fringe-tracker there are four states: (1) Searching, (2) Found, (3) Lock, (4) Lost. The flow-chart for the state-machine is shown in Figure 4. The state-machine begins operating in the “search” state. When a large SNR is found it will enter the “found” state to confirm that the large SNR persists. If it does not it returns to the search mode. If it does persist it enters the “lock” mode. If in “lock” mode the SNR drops low the “lost” state is entered to confirm that the low SNR persists. If large SNR is detected in “lost” mode the state returns to “lock” mode. If the SNR remains low the state switches to “search” mode again. There are two SNR levels in the state machine, the larger  $\text{SNR}_F$ , and the smaller  $\text{SNR}_L$ . Detection of fringes and progression towards the lock state requires SNR to exceed  $\text{SNR}_F$  whereas loss of fringes and progression back to the search state requires SNR to fall below  $\text{SNR}_L$ . This creates a natural hysteresis effect of the fringe tracker and helps ensure that it does not change state too rapidly between the different states. This also makes it easier for the instrument operator to select appropriate SNR thresholds for a particular observing sequence.

## 3. OBSERVING CONFIGURATION

The goal of the project is to produce high-resolution images of stellar surfaces. That requires excellent and wide coverage of the Fourier domain, which in turn requires long and short baselines at all orientations. Baseline bootstrapping provides the long and short baselines. Earth-rotation provides some of the angular rotation of

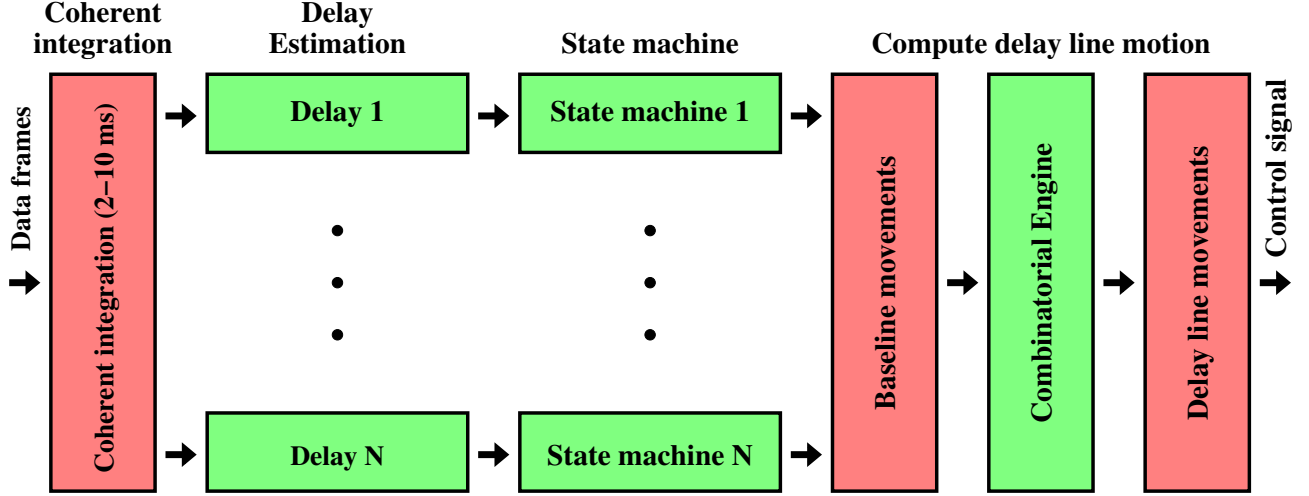


**Figure 3.** Top-level schematic of the New Classic fringe tracker. At the left are the delay estimators, one for each tracked baseline, in the center the state-machines, also one for each tracked baseline. At the right is the combinatorial engine that computes delay-line commands based on the delay-line movements determined from each state-machine. Red boxes represent data and green boxes represent computations.

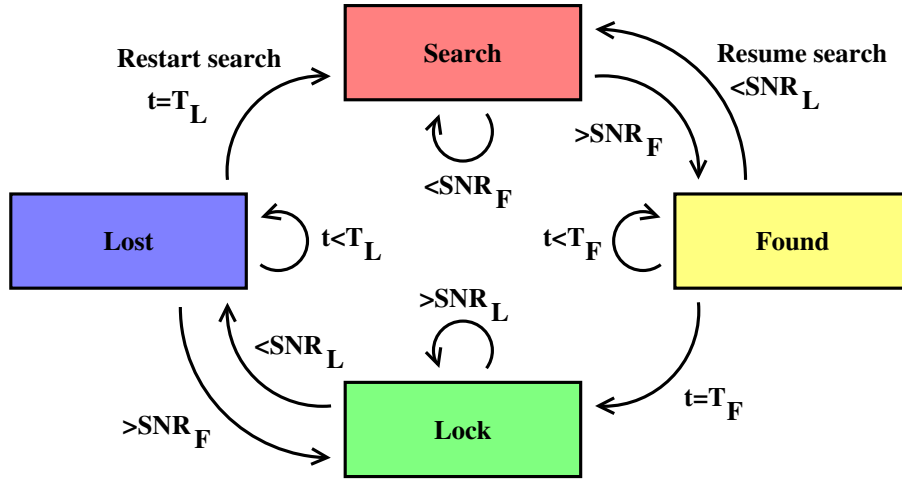


**Figure 4.** The New Classic fringe tracker state machine. The state machine has four states, search, found, lock, lost. A natural progression is from search through found to lock, and then from lock through lost back to search. The found and lost states are used for confirming that fringes are found or lost by temporal correlation. A more detailed explanation of the state machine can be found in section 2.3.

baselines, and picking station sets along the different arms of the Y-shaped NPOI array provides the rest. Figure 5 shows two configurations that we intend to use, the so-called wide configuration (top left) and compact configuration (top right). By carefully arranging the six imaging stations it is possible to create a configuration that makes it possible to switch between the three 6-station chains (red, green, blue) for each of the wide and compact arrays simply by moving relay mirrors in the beam relay pipes and without moving any stations. Because moving relay mirrors is a much faster

operation than moving imaging siderostats it now becomes possible to switch between the three 6-station chains between consecutive observing nights, and thus provide a complete set of observations in as little as 3 nights. These observations then provide a Fourier plane (UV-plane) coverage similar to that illustrated in the bottom panels of Figure 5. These UV-plane coverages assume 6 hours of observations in a night on a single target with 20 minutes between observations. We have previously demonstrated<sup>13</sup> that this observing cadence and associated integration times are realistic for typical

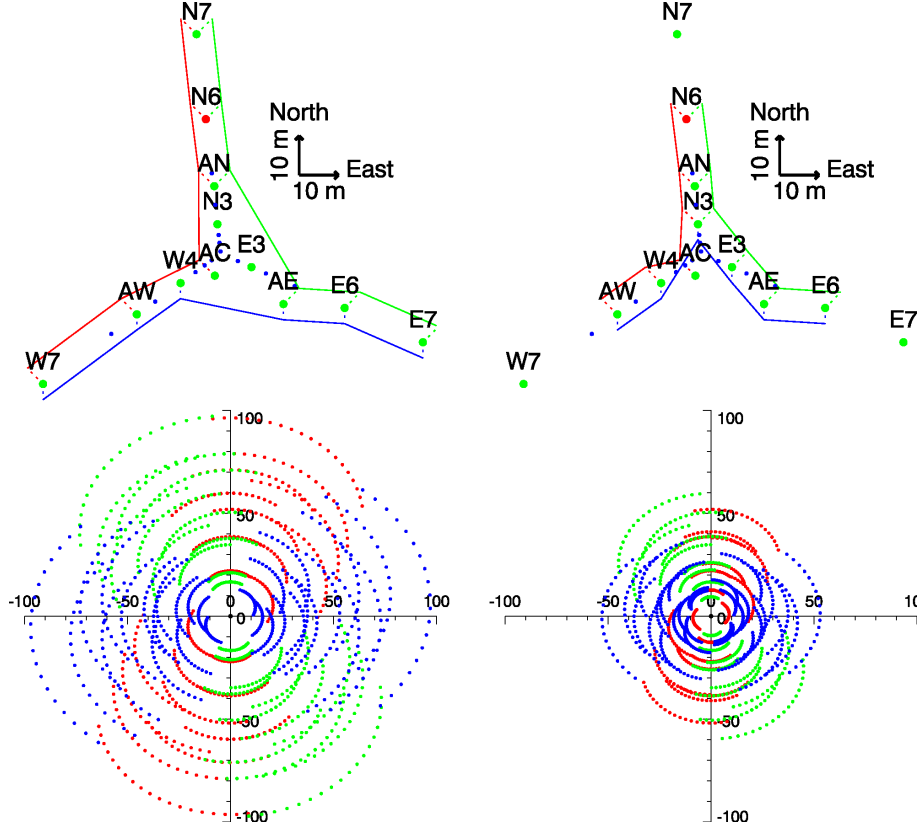


**Figure 5.** Observing configurations. The wide array (left) and the compact array (right). The six imaging stations can be arranged in such a configuration that it is possible to switch between the three different 6-station chains (red, green, blue) while moving only relay and not imaging stations. This makes it possible to switch between the red, green, and blue chains between consecutive observing nights.

stars of magnitude  $V < 6$  at the red end of the spectrum, and approximately  $V < 4$  at the more blue end of the spectrum.

#### 4. INITIAL RESULTS

One of the key capabilities necessary for the NPOI Stellar Surface Imaging Project is the baseline chain bootstrapping. NPOI is unique in that it is the only operating interferometer to have the capability to place six telescopes in a chain. That also means that it is uniquely suited for phasing long baselines that are required for high-resolution imaging. In January 2015 we demonstrated this capability with the New Classic instrument. Because the NPOI is currently undergoing upgrades on its delay-line system only 5 telescope were available at the time of these observations. Nevertheless, even with that reduced functionality at the time, the NPOI still exceeded the capability for baseline bootstrapping of any other interferometer.

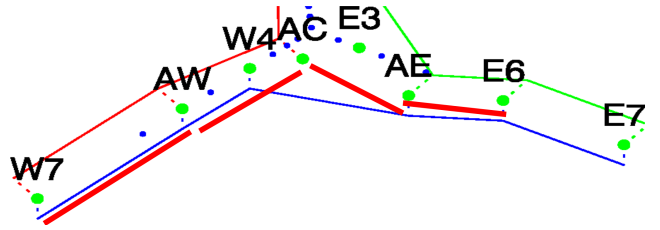


**Figure 6.** The 5-station chain configuration observed in January 2015. The wide red lines mark the short connecting baselines of the configuration. The configuration is similar to the planned blue chain of the wide configuration in Figure 5 but with notable differences discussed in the body of the text.

Figure 6 shows the configuration at the time of the observations in January 2015. The wide red lines mark the short connecting baselines of the configuration. The configuration is similar to the blue chain of the wide configuration in Figure 5. The planned wide configuration is W7-AW-W4-AE-E6-E7, whereas the observed

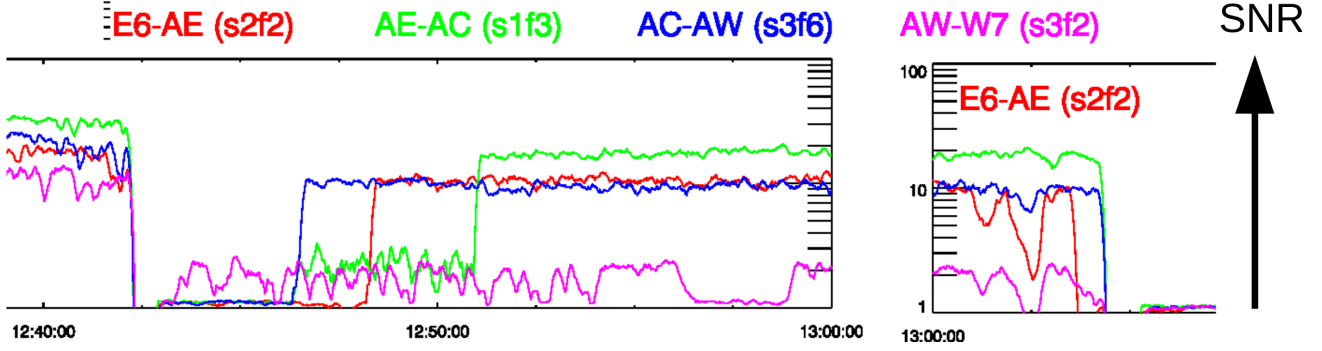


**Figure 7.** This figure is a composite of two sections of the standard SNR summary plot showing a single observation of  $\nu$  UMa, lasting approximately 15 minutes.

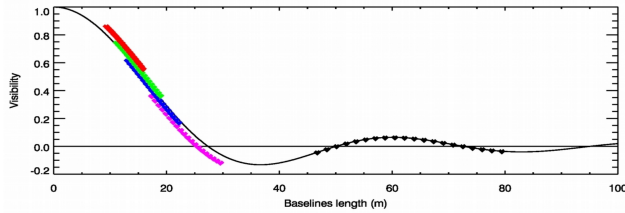


**Figure 8.** The tracking baselines, color-coded as in Figure 7, and the longest bootstrapped baseline, marked in black. The span of the colors covers the wavelength range, with the left end being 850 nm and the right end being 500 nm.

configuration was W7-AW-AC-AE-E6<sup>1</sup>. Essentially we used AC instead of W4 and left out E7. It may seem that it would be more sensible to use AC in the wide configuration anyway because it equalizes the AW-AC and AC-AE baselines better, but the NPOI configuration is not flexible enough for that. The reason is that AC is hard-configured to feed the east arm, and when AE, E6, and E7 are all used there is no room for AC. However because we left out E7 in this observing run we were able to use AC in its place. The observed configuration was not ideal in that it included some short and some long connecting baselines and we were aiming for nearly equal-length connecting baselines. However this represented the best configuration that was available at the time.

This configuration was observed the entire night of January 6, 2015 on a variety of stars with excellent fringe-tracking performance. We tracked fringes on very faint targets. The faintest target observed was HR 3176, a  $V=5.3$  unresolved star. The largest star was  $\nu$  UMa,

<sup>1</sup>The four astrometric stations are AE, AW, AN, and AC for east, west, north, and center, respectively. The imaging stations are named by arm (east, north, or west: E, N, W) and the number of the station along the line (1 is closest to the beam combining lab and 10 is farthest away)

a  $V=3.5$  star with diameter  $d=4.6$  mas. The latter was perhaps the most interesting observation of the night because it demonstrated the high-resolution measurements possible with the 5-telescope bootstrapping configuration (and even larger resolution achievable with 6 telescopes once all are fully operational). The star was so large that the W7-AW baseline contained the nominal first null in the center of the wavelength range making it a challenging fringe-tracking problem. Figure 7 shows the fringe-tracking SNR for the four connecting baselines for an observing interval on the resolved star. The SNR traces are color-coded according to the baselines written at the top of the figure. The fringe tracker was started at approximately 12:43, and almost immediately the W7-AW baseline was captured despite being the faintest. Then followed AC-AW and AE-AC and later E6-AE. Notice that the SNR on AE-AC jumped at about 12:51. This indicates that the baseline was tracking on a side-lobe until that time, something that can occur under large SNR conditions. All baselines, except for W7-AW, showed a very strong fringe-tracking SNR, whereas for W7-AW, the SNR was weak, but clearly distinguishable from noise. Some more manipulation of the SNR thresholds of the fringe-tracker would have resulted in a better track on W7-AW. Nonetheless, under non-ideal conditions all baselines were tracking and data obtained.

To illustrate the importance of this achievement, Figure 8 shows the fringe-tracking baselines overlaid on a nominal 4.6 mas uniform disk model. The tracking baselines are color-coded as in Figure 7, and the longest baselines, W7-E6, is plotted in black. The left-most end of the colored traces corresponds to 850 nm wavelength, and the right-most to 500 nm.

Those observations on January 6, 2015 represent an extremely important achievement on the path to high-resolution interferometric imaging. We demonstrated a

flexible dynamic fringe-tracking system that can be extended to any number of bootstrapped baselines.

## 5. CONCLUSION

The NPOI Stellar Surface Imaging Project is a ambitious project to take full advantage of the NPOI's built-in capabilities to do baseline and wavelength bootstrapping of 6-telescope chains, and rapid reconfiguration of the instrument. The project has achieved an important milestone by demonstrating 5-telescope baselines bootstrapping. The NPOI is the only interferometer to be able to make this demonstration, and 6-telescope bootstrapping will follow as current observatory upgrade work is completed. That can then lead to the observations outlined and the completion of the NPOI Stellar Surface Imaging Project.

## ACKNOWLEDGMENTS

This work is supported by the National Science Foundation under grant AST-1310800, as well as by the Naval Research Laboratory. The NPOI is funded by the Office of Naval Research and the Oceanographer of the Navy.

## REFERENCES

1. J. T. Armstrong, R. B. Hindsley, S. R. Restaino, J. A. Benson, D. J. Hutter, F. J. Vrba, R. T. Zavala, S. A. Gregory, and H. R. Schmitt, "Observations of a geosynchronous satellite with optical interferometry," in Proc. Advanced Maui Optical and Space Surveillance Technologies Conference, 2009.
2. J. T. Armstrong, R. B. Hindsley, S. R. Restaino, R. T. Zavala, J. A. Benson, F. J. Vrba, D. J. Hutter, S. A. Gregory, H. R. Schmitt, J. R. Andrews, and C. C. Wilcox, "Observations of a geosynchronous satellite with optical interferometry," in Adaptive Coded Aperture Imaging, Non-Imaging, and Unconventional Imaging Sensor Systems II, S. Rogers, D. P. Casasent, J. J. Dolne, T. J. Karr, and V. L. Gamiz, eds., p. 78180L, 2010.
3. J. T. Armstrong, R. B. Hindsley, H. R. Schmitt, F. J. Vrba, J. A. Benson, D. J. Hutter, and R. T. Zavala, "Detection of a geostationary satellite with the Navy Prototype Optical Interferometer," in Proc. Optical and Infrared Interferometry II, W. C. Danchi, F. Delplancke, and J. K. Rajagopal, eds., pp. 77343C–77343C–7, 2010.
4. E. J. Bakker, D. A. Klinglesmith, A. M. Jorgensen, D. Westpfahl, V. Romero, and C. Cormier, "Imaging of geostationary satellites with the MRO interferometer," in Proc. Advanced Maui Optical and Space Surveillance Technologies Conference, 2009.
5. A. M. Jorgensen, H. R. Schmitt, D. Mozurkewich, J. T. Armstrong, S. Restaino, and R. L. Hindsley, "Interferometric imaging of geostationary satellites: Signal-to-noise considerations," in Proc. Advanced Maui Optical and Space Surveillance Technologies Conference, 2011.
6. D. Mozurkewich, J. T. Armstrong, R. B. Hindsley, A. M. Jorgensen, S. R. Restaino, and H. R. Schmitt, "An imaging interferometer for compact sources," in Proc. SPIE 8165, 2011.
7. D. Mozurkewich, J. T. Armstrong, R. B. Hindsley, A. M. Jorgensen, S. R. Restaino, and H. R. Schmitt, "Toward the ground-based imaging of satellites at geosynchronous altitude," in Proc. Advanced Maui Optical and Space Surveillance Technologies Conference, 2011.
8. H. R. Schmitt, D. Mozurkewich, S. R. Restaino, J. T. Armstrong, E. K. Baines, R. B. Hindsley, and A. M. Jorgensen, "Simulated synthesis imaging of geostationary satellites," in Proc. Advanced Maui Optical and Space Surveillance Technologies Conference, 2011.
9. J. T. Armstrong, D. Mozurkewich, L. J. Rickard, D. J. Hutter, J. A. Benson, P. F. Bowers, N. M. Elias II, C. A. Hummel, K. J. Johnston, D. F. Buscher, J. H. Clark III, L. Ha, L.-C. Ling, N. M. White, and R. S. Simon, "The navy prototype optical interferometer," The Astrophysical Journal **496**, pp. 550–571, 1998.
10. A. M. Jorgensen, D. Mozurkewich, T. Armstrong, H. Schmitt, C. Gilbreath, R. Hindsley, and T. A. Pauls, "Improved coherent integration through fringe model fitting," Astronomical Journal **134**, pp. 1544–1550, 2007.
11. A. M. Jorgensen, D. Mozurkewich, H. Schmitt, R. Hindsley, J. T. Armstrong, and T. A. Pauls, "Practical coherent integration in optical interferometry," in Proceedings of the SPIE Conference Astronomical Telescopes and instrumentation, 2008.
12. A. M. Jorgensen, H. Schmitt, J. T. Armstrong, D. Mozurkewich, E. Baines, R. Hindsley, D. Hutter, and S. Restaino, "Coherent integration results from the NPOI," in Proceedings of the SPIE meeting Astronomical Telescopes and Instrumentation, 2010.

13. A. M. Jorgensen, D. Mozurkewich, H. R. Schmitt, G. T. van Belle, D. J. Hutter, J. Clark, J. T. Armstrong, E. K. Baines, K. Newman, M. Landavazo, B. Sun, and S. R. Restaino, “Progress toward unprecedented imaging of stellar surfaces with the Navy precision optical interferometer,” in Society of Photo-Optical Instrumentation Engineers (SPIE) Conference Series, Society of Photo-Optical Instrumentation Engineers (SPIE) Conference Series **9146**, p. 0, July 2014.